# Supporting Information

"Insights into the Mechanism of Proton Transport in Cytochrome c Oxidase"

Takefumi Yamashita and Gregory A. Voth

*Department of Chemistry, James Franck Institute, Institute for Biophysical Dynamics, and Computation Institute, University of Chicago, 5735 S. Ellis Ave., Chicago, Illinois 60637, USA*

In this Supporting Information (SI), detailed data are given to support the discussion of the main text. In the first section, snapshots of the characteristic hydrogen bond networks are shown. In the second, the PMF curves are given for less realistic CcO models and then the underlying physics are discussed. Finally, methodological details including the protonatable heme model are given in the last section.

## 1. Effect of oxidation state change on the hydrogen bond network

### 1.1 Case of protonated Glu242

In order to explain the oxidation state dependence of the PMF curve along the proton-pumping pathway, several typical hydrogen networks around the pumped protons are shown in Figs. S1 and S2. Whereas the water cluster is localized around PRDa3 in the RO state, it is observed that the OO and OR states form a hydrogen-bonded water chain between the BNC and PRDa3. This water chain also binds the excess proton bound by PRDa3. Forming such a water chain in the OR state may be important for the scalar proton to transport to the BNC in the oxidative phase. Although the present BNC models are more closely related to the reductive phase where the scalar proton is transported through the K-channel, such a hydrogen bond chain can be still observed between the BNC and the protonated PRDa3.

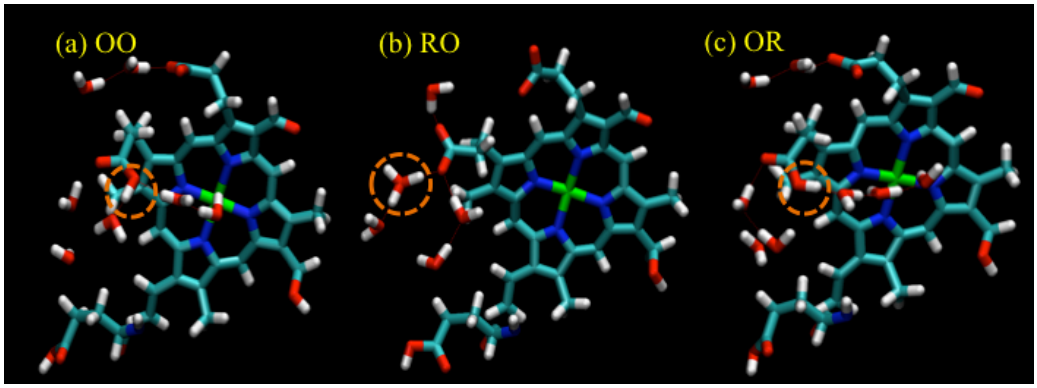


Figure S1: Hydrogen bond network in CcO(I+II) of which the BNC binds a water molecule. Orange circles highlight the most protonated species. To simplify the pictures, water molecules within 10 Å of the excess proton CEC are shown. The excess proton CEC is located at (a) $z_{CEC}$ = 6.6, (b) 6.8, and (c) 6.5 Å.

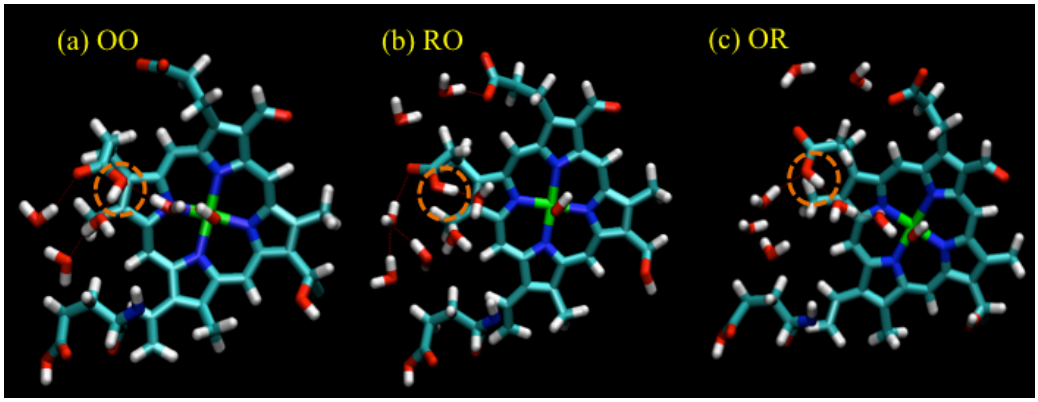


Figure S2: Hydrogen bond network in CcO(I+II) of which BNC binds a hydroxide anion. Orange circles highlight the most protonated species. To simplify the pictures, water molecules within 10 Å of the excess proton CEC are shown. The excess proton CEC is located at (a) $z_{CEC}$ = 6.6, (b) 7.4, and (c) 7.0 Å.

**1.2 Case of deprotonated Glu242**

Figure S3 shows typical snapshots of the non-polar cavity near the minimum of PMFs. It is observed that

Glu242 turns up and stabilizes the excess proton in the non-polar cavity. Such a conformational change affects the hydrogen bond network in the non-polar cavity. In this case, a hydrogen-bonded water chain can be seen from the BNC even in the RO state. However, the other terminal is the up-conformation Glu242 and thus PRDa3 and the excess proton are not included in this hydrogen-bonded chain. In the OO and OR state, PRDa3 and the excess proton are closely bound to the water chain connecting to the BNC as in the protonated Glu242 cases.

Glu242 turns down only in the case of the RO state and loses the direct electrostatic attraction to the excess proton above the region of $z_{\mathrm{CEC}} \approx 9$ Å (see Fig. S4). Accordingly, the PMF becomes flat around this region (see Fig. 5 of the main text). In contrast, the up-conformation of the Glu242 is kept in the whole region in the OO and OR states, and contributes the increase of the PMF even in the region of $z_{\mathrm{CEC}} \geq 9$ Å.

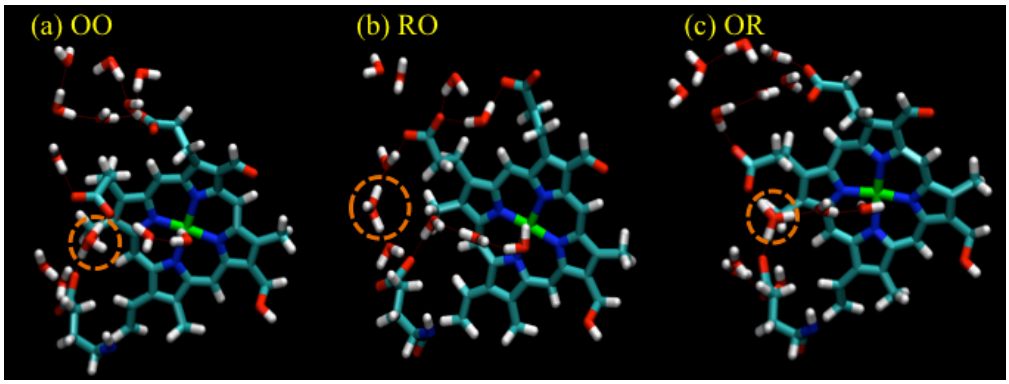


Figure S3: Hydrogen bond network in CcO(I+II) of which BNC binds a water molecule. Orange circles highlight the most protonated species. To simplify the pictures, water molecules within 10 Å of the excess proton CEC are shown. The excess proton CEC is located at (a) $z_{\mathrm{CEC}}$ = 5.8, (b) 6.1, and (c)7.1 Å.

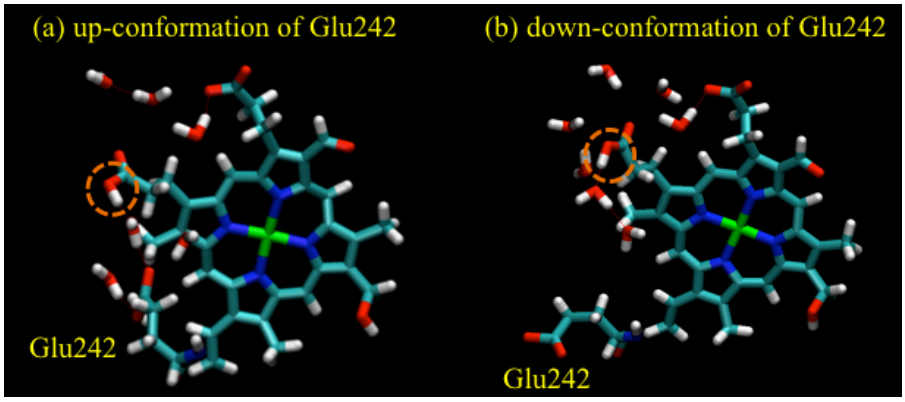


Figure S4: Snapshots of the hydrogen bond network around the excess proton in the CcO(I+II) model. Here, Glu242 is deprotonated and a water molecule is bound at the BNC. Orange circles highlight the most protonated species. To simplify the pictures, water molecules within 6.5 Å of the excess proton CEC are shown. The excess proton CEC is located at (a) $z_{CEC}$ = 8.4 and (b) 9.2 Å.

**2. Less realistic CcO models**

In this work, the clear oxidation state dependence of the proton transport is elucidated with a reasonably realistic CcO environment, which includes SU-II and the protonatable PRDa3. In this section, more information is extracted by comparison with results for less realistic reduced CcO models.

First, the effect of the protonation of PRDa3 is discussed. As shown in Fig. S5(a) and (b), the PMFs are largely affected by prohibiting the protonation of PRDa3. This result suggests that the protonated state of PRDa3 influences the hydrogen bond network in the non-polar cavity and the valid description of the protonation is necessary to study the proton transport around the non-polar cavity.

Next, SU-II is removed to see the effect of that subunit. As shown in Fig. S5(c), the SU-II effect is even larger and the PMFs for OO and OR becomes exothermic, although they are endothermic in the CcO(I+II) model. In addition, the sensitivity of PMFs to the oxidation state decreases. As shown in Fig. S5(d), the sensitivity becomes even less, if the protonation of PRDa3 is forbidden. This unprotonatable CcO(I) model is basically equivalent to

the model used in a previous study.[1] Therefore, removing these two important factors can be considered to be the main reason why sufficiently large dependence on the oxidation state could not be observed in that previous study. Note that the difference between the PMFs of the previous study and those in Fig.S5(d) is caused by the difference of the on-site charge values of the $Cu_B$ center. In particular, one N site of His291 is much less negatively charged in this work, and therefore the PMF curves become more exothermic.

To discuss the effect of SU-II in more detail, a typical snapshot of the CcO(I) model is compared to that of the CcO(I+II) model. As shown in Fig. S6, more water molecules (inside the yellow circle) can be observed in the absence of SU-II than in the presence of SU-II. These additional water molecules can stabilize the proton above the PRDa3 and thus enhance the proton escape from the non-polar cavity. This is probably the main reason why the PMFs become more exothermic in the absence of SU-II. Although the other effects such as the direct electrostatic interaction from the SU-II and the constraints of the SU-I/SU-II interface are not excluded, such an effect of the additional water molecules should be dominant. Furthermore, the hydrogen-bond network below PRDa3 is also affected and the water chain between the BNC and PRDa3 disappear in the CcO(I) model. Thus, the oxidation state dependence of the PMF curve becomes significantly smaller in the CcO(I) model.

Finally, it is worth noting that the experimental results on mutating Arg438 (corresponding to Arg481 in *R. Sphaeroides*) show that the mutation is not effective enough to prohibit the proton pumping but affects the proton pumping efficiency to some extent.[2,3] This result indicates that the mutation influences the hydrogen bond network in the region between the down-conformation PRDa3 and Arg438 (yellow circle in Fig. S6), but not drastically.

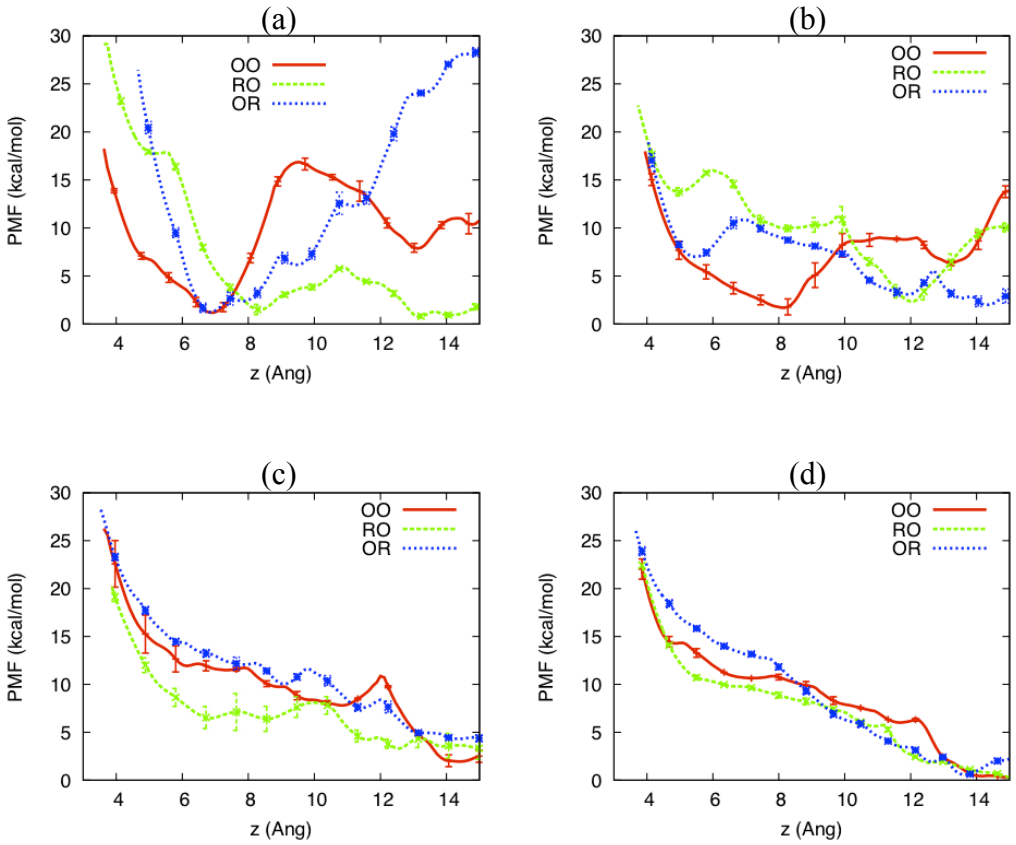


Figure S5: Free energy profiles (PMFs) for (a) the protonatable CcO(I+II) model (This is the same as Fig. 4 in the main text), (b) the unprotonatable CcO(I+II) model, (c) the protonatable CcO(I) model, and (d) the unprotonatable CcO(I) model. In all the cases, the BNC binds a water molecule and Glu242 is protonated.

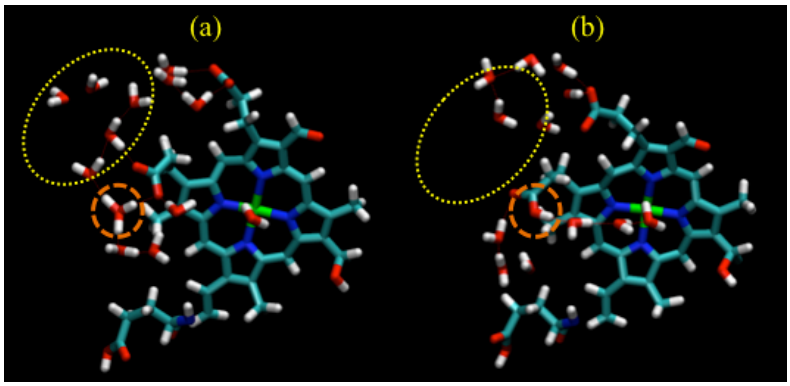


Figure S6: The water molecules within 10 Å of the excess proton CEC are shown for the OR state of (a) the CcO(I) model and (b) the CcO(I+II) model. Orange circles highlight the most protonated species. The excess proton CEC is located at (a) $z_{CEC}$ = 6.1 and (b) 6.9 Å.

**3. Methodological Details**

Due to Grotthuss shuttling one cannot assign a specific hydrogen nucleus to the "excess proton". Thus, to describe the position of the protonic charge defect, the center of excess charge (CEC), defined as[4,5]

$$\mathbf{r}_{\mathrm{CEC}} = \sum_i |c_i|^2 \, \mathbf{r}_i^{\mathrm{COC}} \tag{1}$$

is adopted in this paper. Here, the $\mathbf{r}_i^{\mathrm{COC}}$ is the center of charge of the protonated molecular species in the *i*-th EVB basis state and the $c_i$ is the corresponding element of the ground state eigenvector of the EVB matrix.

The standard AMBER force field[6] was employed to describe CcO. The partial charges of two heme groups were the same as in the paper of Xu and Voth,[1] whereas the charges of $Cu_A$ and $Cu_B$ are taken from the paper of Tashiro and Stuchebrukov.[7] In the $OH^-$-bound CcO model, Mulliken charge analysis was employed to estimate the charge transfer from the hydroxide to heme $a_3$ ring. The MS-EVB2 model[8] was employed to describe the protonated water cluster in CcO. The protonatable PRDa3 model was constructed based on quantum chemical calculations [see Refs. 9 and 10]. The MS-EVB program based on DL_POLY was generalized to allow both of the oxygen sites of the carboxylate to be protonatable in this work. The α-carbon of all of the residues and the long tails of the heme groups were tethered to the crystal structure geometries [PDB code 1V54][11] with harmonic constraints ($k = 1$ kcal/mol/Å$^2$). All of the quantum chemical calculations were performed with the Gaussian 03 software package.[12]

The protonatable propionate model was constructed within the framework of the MS-EVB method by

following the procedure of Maupin *et al.*[9] Force field parameters were fitted to the potential energies from DFT/B3LYP electronic structure calculations. Then, one parameter ($V_{ii}^0$) was slightly adjusted so that the p$K_a$ value calculated through the MD simulations in the bulk water agree better with the experimental value. The parameters are tabulated in Table S1, where the parameters are defined as in the paper of Maupin *et al.*[9] Figure S7(a) shows that the PMFs for the protonation of propionate in the bulk water as a function of the distance ($r$) between the excess proton CEC and the protonatable oxygen site. The global minimum located at $r \approx 0.5$ Å corresponds to the protonated propionate, whereas the minimum at $r \approx 2.5$ Å corresponds to the contact ion pair. The p$K_a$ value calculated from this PMF (4.90±0.01) agrees well with the experimental value (4.87).

The protonatable heme model can be obtained by linking the propionate model to the D-position of the heme ring. The PMF for the protonation of heme is also given in Fig. S7(a). Here, heme is in the bulk water not in the CcO environment, and the long alkyl chain and A-propionate are replaced by the hydrogen atoms for simplicity. Due to the electrostatic repulsion between the excess proton and the heme ring, the protonated state is destabilized. Thus, when the heme is oxidized, it is more destabilized. (The calculated p$K_a$ values are 2.35±0.01 and 0.04±0.03 for the reduced and oxidized states, respectively.) Such sensitive dependence of the protonation on the electrostatic environment motivates one to investigate the effect of the PRDa3 protonation in the realistic CcO environment.

Finally, to characterize the delocalization of the excess proton charge defect, the $|c_{\max}|^2$ distribution was calculated as a function of $r$. Thus, the two-dimensional distribution function was normalized for each $r$ value. As shown in Fig. S7(b-d), the delocalization state of the protonic charge is not largely affected by the heme group, although the PMF is significantly changed. (In fact, the charge defect delocalization is found slightly perturbed by the heme ring only at $r \approx 4$ Å.)

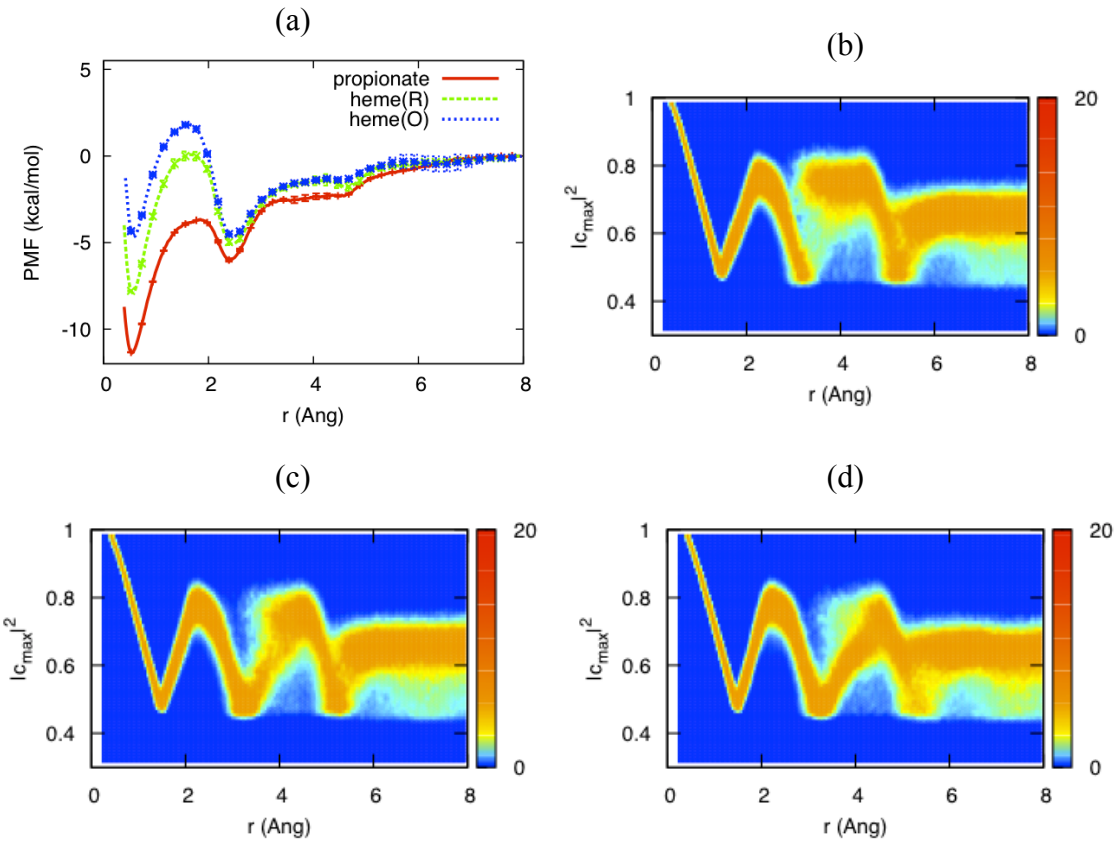


Figure S7: (a) Free energy profiles (PMFs) as functions of distance between the excess proton CEC and the protonatable oxygen site. Distributions of the largest MS-EVB state population for (b) the propionate, (c) the reduced heme [heme(R)], and (d) the oxidized heme [heme(O)], respectively.

Table S1: Parameters of the protonatable propionate model

| Parameter | Value | Parameter | Value |
|---|---|---|---|
| $V_{ii}^{0}$ | -110.53 kcal/mol | $\beta$ | -1.615 Å$^{-2}$ |
| $V_{ij}^{\text{const}}$ | -31.51 kcal/mol | $b_{\text{DA}}$ | 2.506 Å |
| $r_{sc}^{0}$ | 1.02 Å | $\varepsilon$ | 1.70 Å$^{-1}$ |
| $\lambda$ | -0.183 | $c_{\text{DA}}$ | 2.58 Å |
| $R_{\text{DA}}^{0}$ | 2.89 Å | $\gamma$ | 5.25 Å$^{-2}$ |
| $C$ | 0.8179 | $a_0$ | 143.48 kcal/mol |
| $\alpha$ | 0.202 Å$^{-2}$ | $a_1$ | 1.98 Å$^{-1}$ |
| $a_{\text{DA}}$ | 2.47 Å | $a_2$ | 1.00 Å |

**References:**


(1) Xu, J.; Voth, G. A. *Biochim. Biophys. Acta-Bioenerg.* **2008**, *1777*, 196-201.

(2) Lee, H. J.; Ojemyr, L.; Vakkasoglu, A.; Brzezinski, P.; Gennis, R. B. *Biochemistry* **2009**, *48*, 7123-7131.

(3) Egawa, T.; Lee, H. J.; Gennis, R. B.; Yeh, S. R.; Rousseau, D. L. *Biochim. Biophys. Acta-Bioenerg.* **2009**, *1787*, 1272-1275.

(4) Voth, G. A. *Accounts Chem. Res.* **2006**, *39*, 143-150.

(5) Swanson, J. M. J.; Maupin, C. M.; Chen, H. N.; Petersen, M. K.; Xu, J. C.; Wu, Y. J.; Voth, G. A. *J. Phys. Chem. B* **2007**, *111*, 4300-4314.

(6) Cornell, W. D.; Cieplak, P.; Bayly, C. I.; Gould, I. R.; Merz, K. M.; Ferguson, D. M.; Spellmeyer, D. C.; Fox, T.; Caldwell, J. W.; Kollman, P. A. *J. Am. Chem. Soc.* **1995**, *117*, 5179-5197.

(7) Tashiro, M.; Stuchebrukhov, A. A. *J. Phys. Chem. B* **2005**, *109*, 1015-1022.

(8) Day, T. J. F.; Soudackov, A. V.; Cuma, M.; Schmitt, U. W.; Voth, G. A. *J. Chem. Phys.*

**2002**, *117*, 5839-5849.

(9) Maupin, C. M.; Wong, K. F.; Soudackov, A. V.; Kim, S.; Voth, G. A. *J. Phys. Chem. A* **2006**, *110*, 631-639.

(10) Yamashita, T.; Voth, G. A. *J. Phys. Chem. B* **2010**, *114*, 592-603.

(11) Tsukihara, T.; Shimokata, K.; Katayama, Y.; Shimada, H.; Muramoto, K.; Aoyoma, H.; Mochizuki, M.; Shinzawa-Itoh, K.; Yamashita, E.; Yao, M.; Ishimura, Y.; Yoshikawa, S. *Proc. Natl. Acad. Sci. U. S. A.* **2003**, *100*, 15304-15309.

(12) Frisch, M. J.; Trucks, G. W.; Schlegel, H. B.; Scuseria, G. E.; Robb, M. A.; Cheeseman, J. R.; Montgomery, J., J. A.; Vreven, T.; Kudin, K. N.; Burant, J. C.; Millam, J. M.; Iyengar, S. S.; Tomasi, J.; Barone, V.; Mennucci, B.; Cossi, M.; Scalmani, G.; Rega, N.; Petersson, G. A.; Nakatsuji, H.; Hada, M.; Ehara, M.; Toyota, K.; Fukuda, R.; Hasegawa, J.; Ishida, M.; Nakajima, T.; Honda, Y.; Kitao, O.; Nakai, H.; Klene, M.; Li, X.; Knox, J. E.; Hratchian, H. P.; Cross, J. B.; Bakken, V.; Adamo, C.; Jaramillo, J.; Gomperts, R.; Stratmann, R. E.; Yazyev, O.; Austin, A. J.; Cammi, R.; Pomelli, C.; Ochterski, J. W.; Ayala, P. Y.; Morokuma, K.; Voth, G. A.; Salvador, P.; Dannenberg, J. J.; Zakrzewski, V. G.; Dapprich, S.; Daniels, A. D.; Strain, M. C.; Farkas, O.; Malick, D. K.; Rabuck, A. D.; Raghavachari, K.; Foresman, J. B.; Ortiz, J. V.; Cui, Q.; Baboul, A. G.; Clifford, S.; Cioslowski, J.; Stefanov, B. B.; Liu, G.; Liashenko, A.; Piskorz, P.; Komaromi, I.; Martin, R. L.; Fox, D. J.; Keith, T.; Al-Laham, M. A.; Peng, C. Y.; Nanayakkara, A.; Challacombe, M.; Gill, P. M. W.; Johnson, B.; Chen, W.; Wong, M. W.; Gonzalez, C.; Pople, J. A. In Gaussian, Inc.: Wallingford CT, 2004.